

EFFECT OF ANGLE OF ATTACK KINEMATICS ON PASSIVE FLAPPING FOIL POWER GENERATION

John Young and Joseph C.S. Lai
School of Engineering and Information Technology
University of New South Wales, Canberra, ACT, 2600, Australia

Keywords: *flapping foil, power generation*

Abstract

A fully passive flapping foil turbine was simulated using a 2D Navier Stokes solver with two-way fluid structure interaction at a Reynolds number of 1100. The angle of attack profile was specified, and variations in the phase and shape of this profile on the power generation efficiency investigated. Performance was found to be most sensitive to the phase, with relatively lesser effects from variations in the angle of attack during the periods outside stroke reversal. This behaviour was determined chiefly by the timing of the interaction of a large leading edge vortex with the trailing edge of the foil.

1 Introduction

Flapping foils are under active consideration as an alternative to traditional rotary turbines, for power generation in wind, tidal and oceanic currents, and rivers (e.g. [1-4]), following an approach pioneered by McKinney and DeLaurier [5]. In this concept an oscillating pitch motion creates a fluid dynamic force on the foil, which then translates in an oscillatory manner in response. Power is typically extracted from this translational (plunge) motion, and performance is measured as for rotary turbines, that is as the percentage of energy extracted from the fluid stream passing through the frontal area of the turbine (in this case the swept area of the foil).

Such power generation mechanisms promise a number of potential advantages in comparison to rotary turbines, including a relatively low foil maximum speed which is

expected to diminish the impact on wildlife. This is due to the entire foil moving at the same speed, thereby increasing the proportion of the turbine area working at maximum power extraction. In the tidal flow and river applications, operation is also possible in shallower water than for horizontal axis rotary turbines, when the foil is oriented horizontally and plunges vertically. Here the turbine size may be increased by extending the foil span, without affecting the plunge motion amplitude.

A number of different factors affecting performance have been investigated in recent times, including foil shape (e.g. [6]), laminar versus turbulent flow conditions (e.g. [2,3]), operation in a shear flow [4], and activation strategy. The latter describes the manner in which the foil is driven, and may be broadly classified as fully prescribed, partially passive or fully passive.

In fully prescribed studies both the plunging and pitching motions are given as functions of time. In partially passive strategies only the pitching motion is typically prescribed (e.g. [7,8]), where some of the power extracted from the plunge motion is diverted to drive a pitch motor, and thus the pitch motion is indirectly flow-driven. Fully passive strategies rely on fluid-structure interaction to determine both the plunging and pitching motions (e.g. [2,9,10]). Such systems may alternatively be classified in terms of the degrees of freedom and the constraints on the motion, e.g. 2-dof, strongly constrained pitch motion, loosely constrained plunge motion [8]; 1-dof, fully constrained plunge and pitch motions [11]; or 1-dof, loosely constrained pitch and plunge motions [2,10].

In all these studies flapping kinematics is a primary determinant of performance (that is, greatest extraction of power from the available fluid stream) [1]. Most studies have considered sinusoidal profiles in both pitch and plunge, although some have studied the effect of non-sinusoidal profiles.

Ashraf et al. [12] and Platzer et al. [13] considered prescribed motion for single foils and two foils in a tandem arrangement, for sinusoidal and non-sinusoidal oscillations, a range of different phases between pitch and plunge, different phases between front and rear foils, and different spacing between the foils. For non-sinusoidal motion, the pitch rotation of the foil was compressed so that it occurred at the top of the upstroke and bottom of the downstroke with periods of constant pitch angle in between. This increased the power output by up to 17% over sinusoidal motions, by presenting the foil to the flow with the highest angle for a greater proportion of the flapping stroke than for sinusoidal motion. Similarly Xiao et al. [14] simulated $Re = 1.0 \times 10^4$ flow over a NACA0012 foil. They explored the effect of different periods of constant pitch angle, and predicted similar performance increases as seen by [12,13].

Hover et al. [15] noted that a quasi-steady consideration of the kinematics leads to the conclusion that the angle of attack should be held at the largest possible value for the longest possible time throughout the flapping cycle, to create the largest time-averaged aerodynamic forces. While this was in the context of flapping foil propulsion, it is also applicable to power generation. This may be seen in Fig. 1, where the phase of the angle of attack relative to the plunge motion is the determinant of whether the foil produces thrust or power. It is therefore natural to explore the effect of the angle of attack trajectory (i.e. time history) for the power generation problem, particularly noting that this application has been shown to be highly unsteady and dependent on the formation, evolution and interaction of LEVs [1,2], which are in turn sensitive to angle of attack.

This work extends a previous study by Young et al. [2] on a fully passive turbine design (that is, both plunging and pitching of the

foil are driven directly by fluid-structure interaction). Maintaining a given angle of attack time history was shown to provide a significant benefit in efficiency compared to controlling the pitch angle without consideration of the angle of attack (41% versus 30% for the conditions considered). This work investigates the effect of variations in the angle of attack time history. The aim is not finding the optimum angle of attack profile per se (which will be dependent on a wide range of factors including Reynolds number, foil geometry and plunge amplitudes), rather it is about investigating the effect of changes in the profile on the flow physics, to understand the sensitivity of the power output to these changes as a first step towards developing a robust control system.

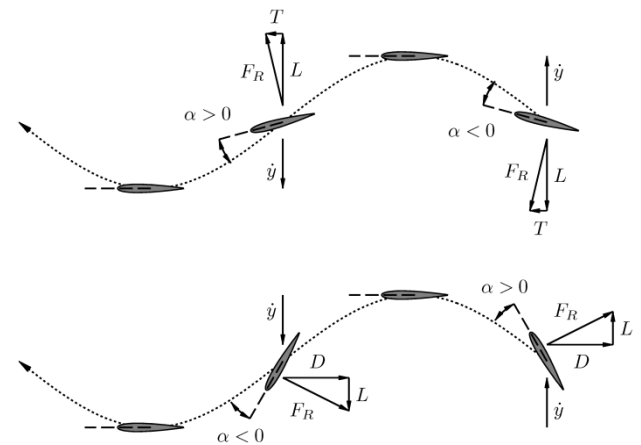


Fig. 1. Regimes of operation of a flapping foil, and the associated angle of attack and force directions throughout the flapping cycle. Top: propulsion mode. Bottom: power generation mode. Adapted from [16,17].

2 Flapping Foil Kinematics

2.1 Foil Motion

The flapping wing turbine is modeled as a two-dimensional foil undergoing both pitching and plunging motions. The motion is defined by plunge position y and pitch angle θ , as shown in Fig. 2. The angle of attack of the foil is given by:

$$\alpha = \theta - \tan^{-1} \frac{\dot{y}}{U_\infty} \quad (1)$$

The plunge and pitch motion are linked to the rotation of a flywheel as in Young et al. [2], so that the system is reduced from 2-dof (pitch and plunge) to 1-dof (flywheel angle). Power extraction from the system is modeled as a viscous damper attached to the flywheel. The equation of motion of the combined foil-flywheel system is determined via the conservation of energy as:

$$m_{foil}\dot{y}\ddot{y} + I_{foil}\dot{\theta}\ddot{\theta} + I_{fly}\dot{\beta}\ddot{\beta} = L\dot{y} + M\dot{\theta} - c_{fly}\dot{\beta}^2 \quad (2)$$

where β is the flywheel angle, I_{foil} is the foil inertia measured about the pivot point, I_{fly} is the flywheel inertia measured about its centre, and c_{fly} is the viscous damper strength.

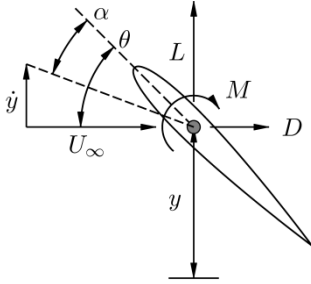


Fig. 2. Plunging motion y and pitching motion θ of the foil, and the associated angle of attack. Lift L , drag D and moment M about the pivot point also shown.

In what follows, the plunge motion y and angle of attack α are specified as functions of the flywheel angle β rather than as functions of time, and the pitch angle θ is determined from Eq. (1), which may be recast as:

$$\theta(\beta) = \alpha(\beta) + \tan^{-1} \frac{y_\beta \dot{\beta}}{U_\infty} \quad (3)$$

where $y_\beta = \partial y / \partial \beta$. The equation of motion is solved in terms of β :

$$\ddot{\beta} = \frac{1}{m_{foil}(y_\beta)^2 + I_{foil}(\theta_\beta)^2 + I_{fly}} [Ly_\beta + M\theta_\beta - c_{fly}\dot{\beta} - (m_{foil}y_\beta y_{\beta\beta} + I_{foil}\theta_\beta \theta_{\beta\beta})\dot{\beta}^2] \quad (4)$$

where time derivatives of y and θ are converted to time derivatives of β , i.e. $\dot{y} = y_\beta \dot{\beta}$, $\dot{\theta} = \theta_\beta \dot{\beta}$. The term $Ly_\beta + M\theta_\beta$ in Eq. (4) represents the

fluid dynamic torque transmitted to the flywheel by the mechanism linking the pitch and plunge motions to the flywheel rotation.

The power output of the turbine is measured as the time-average of the rate of energy dissipation in the flywheel damper:

$$P = \frac{1}{T} \int_t^{t+T} c_{fly} \dot{\beta}^2 dt \quad (5)$$

The efficiency η is determined in the usual manner via comparison with the available power in the flow passing through the frontal area swept by the foil (the 'Betz power'), where unit span s is assumed, and d is the total excursion of the trailing or leading edges of the foil, whichever is greater:

$$P_a = \frac{1}{2} \rho U_\infty^3 s d \quad (6)$$

$$\eta = \frac{P}{P_a} \quad (7)$$

2.2 Angle of Attack Profile

The angle of attack profile is created as a piecewise continuous polynomial in β parameterised in such a way as to generate a wide range of possible profiles, from a sinusoid to a square wave. The profile consists of two second-order (i.e. parabolic) polynomial sections, with position, slope and curvature specified as parameters. The parabolic sections are linked by sixth-order polynomials matched to the parabolic section endpoints position, slope and curvature, and thus are fully constrained once the parabolic parameters have been specified. This is shown in Fig. 3. Here values of 0th, 1st and 2nd derivative at points C and B', and 0th derivative at point D, give seven conditions requiring a sixth order polynomial passing through C-D-B'. Note that α_e is not the maximum angle of attack achieved in the profile, rather it is the amplitude of the equal area sinusoid. This was chosen as a way to normalise different profiles with a range of parameters.

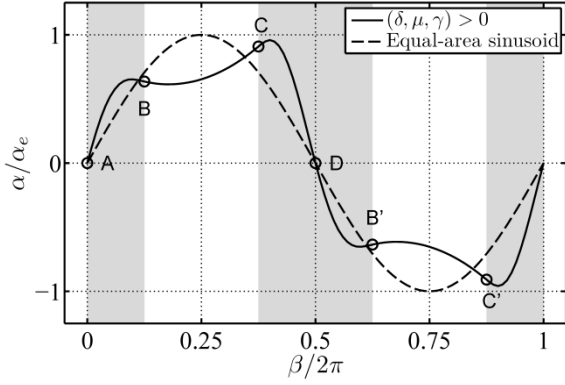


Fig. 3. Angle of attack profile parameterisation via patched polynomials. Points A - D indicate control points, shaded sections indicate sixth-order polynomial, unshaded sections indicate second-order polynomial, δ , μ and γ defined in the text. Points B' and C' are the inverse of B and C, displaced by $\beta/2\pi = 0.5$.

The three parameters controlling the parabolic section width, slope and curvature, δ , μ and γ are defined as follows:

$$\delta = \frac{\beta_C - \beta_B}{\beta_D - \beta_A} = (\beta_C - \beta_B)/\pi \quad (8)$$

$$\mu = \frac{1}{\alpha_e} \frac{\alpha_C - \alpha_B}{\beta_C - \beta_B} = \frac{1}{\pi\delta} \frac{\alpha_C - \alpha_B}{\alpha_e} \quad (9)$$

$$\gamma = \frac{1}{\alpha_e} \left. \frac{\partial^2 \alpha}{\partial \beta^2} \right|_{\beta=\pi/2} \quad (10)$$

The width parameter δ thus represents the duration of the parabolic section of the profile, compared to a half-cycle of foil motion. The slope parameter μ is the slope of the line connecting the endpoints of the parabolic section, non-dimensionalised against the maximum slope of the equal-area sinusoid. The curvature parameter γ is the curvature of the parabolic section, non-dimensionalised against the maximum curvature of the equal-area sinusoid. Positive values indicate a concave up curvature in the first half of the stroke as shown in Fig. 3.

A wide range of angle of attack profiles may be generated with this methodology, as illustrated in Fig. 4. Here the phase by which the angle of attack leads the plunge motion, $\phi = 0.0^\circ$ for all cases. In the top frame of Fig. 4 the width δ is seen to control the 'squareness' of the profile. For $\delta = 0.0$, $\mu = 0.0$ and $\gamma = -1.0$ gives a curve which very closely approximates a

sinusoid (goodness of fit coefficient of determination $R^2 = 0.9999995$ and root mean square error $RMSE = 4.984 \times 10^{-4}$ radians for amplitude $\alpha_e = 1.0$ radians).

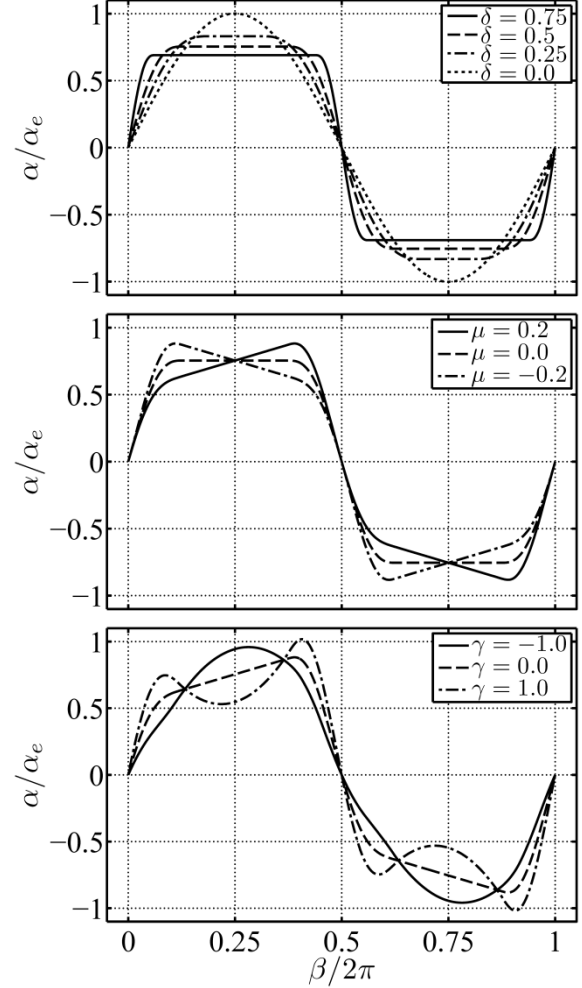


Fig. 4. Effect of width, slope and curvature parameters on angle of attack profiles. Top: width δ variation, $\mu = 0$ and $\gamma = 0$ for all cases (except $\delta = 0$ where $\gamma = -1.0$ which represents a sinusoidal profile). Middle: slope μ variation, $\delta = 0.5$ and $\gamma = 0$ for all cases. Bottom: curvature γ variation, $\delta = 0.5$ and $\mu = 0.2$ for all cases. All profiles have equal magnitude α_e .

The slope μ determines whether the angle of attack peaks early or later in the half-cycle, and the curvature γ controls the nature of the peaks. With positive curvature $\gamma > 0$ profiles with two peaks and a trough per half-cycle are generated, which is characteristic of the angle of attack profile experienced by a flapping foil undergoing sinusoidal plunging and sinusoidal pitching where the plunge velocity is sufficiently high (e.g. [14]). Thus a relatively simple parameterisation allows examination of

widely varying angle of attack profiles and hence flow physics.

3 Numerical Method

The 2D unsteady incompressible Navier Stokes equations, coupled to the flywheel equation of motion, are solved using two-way fluid-structure interaction (FSI) within the commercial computational fluid dynamics (CFD) package Fluent 14.5. The domain is a rectangle with boundaries 20 chords from the foil. Velocity is imposed on the upstream, top and bottom boundaries, and pressure on the downstream boundary. A second-order upwind spatial discretisation is used, and the motion of the foil is introduced via a source term in the Navier Stokes equations for the plunge motion, and rotation of a circular zone around the foil for the pitching motion.

The foil is a NACA0012 section, pivoted at the midpoint of the chord. The flywheel equation of motion Eq. (4) is reduced to a system of first-order ordinary differential equations and discretised in time with a second-order Crank-Nicolson scheme. Details may be found in Young et al. [2], which also contains details of the mesh and time-step refinement, and validation against results in the literature, that was carried out for laminar ($Re = 1100$) and turbulent ($Re = 5.0 \times 10^5$ and 1.1×10^6) conditions. Based on this study, the laminar simulations herein use a time-step of $\Delta t = 1.25 \times 10^{-3}$ seconds and a mesh of 186,000 cells (400 cells on the foil surface) with first cell height from the foil surface of $\Delta = 1.0 \times 10^{-4}$ chords, resulting in a cell Reynolds number $Re_c = 0.2 - 1.2$ on the foil surface at all times. This mesh provided excellent agreement with the time history of aerodynamic forces for the optimum prescribed-motion case of Kinsey and Dumas [17].

4 Results

4.1 Baseline Comparison Case

A baseline angle of attack profile was constructed from the optimal case in Young et al. [2]. In that case, the plunge motion was

given by $y = hc \sin \beta$, with $h = 1.0$, and the angle of attack profile consisted of periods of constant angle of attack α_0 on the upstroke of the foil and $-\alpha_0$ on the downstroke, separated by patched sinusoidal curves for the foil reversals periods. The phase of the angle of attack variation relative to the plunge motion was $\phi = 90^\circ$. For the optimal case from [2], the maximum angle of attack was $\alpha_0 = 40^\circ$ and the 'stroke reversal fraction' $\Delta \hat{\beta}_R$, representing the fraction of the total flapping cycle over which the foil reverses angle of attack, was $\Delta \hat{\beta}_R = 0.2$ (where 0.1 represents rapid reversal and 0.5 represents fully sinusoidal variation).

The baseline profile was created by setting $\mu = 0$ and $\gamma = 0$, and applying a least-squares fit to the Young et al. [2] case letting δ vary. This resulted in a value of $\delta = 0.5337$, with goodness of fit $R^2 = 0.999973$ and $RMSE = 0.186^\circ$. The equal-area sinusoid magnitude was then determined to be $\alpha_e = 53.676^\circ$. This is shown in Fig. 5. The patched polynomial approach has the advantage that the second derivative of the angle of attack profile can be made continuous, as seen in the lower frame of Fig. 5.

The baseline case was compared to the optimum case from [2] at Reynolds number $Re = 1100$, to assess the effect of changing the angle of attack profile from a patched sinusoidal profile (discontinuous in second derivative $\alpha_{\beta\beta}$) to a patched polynomial profile (continuous in second derivative, as shown in Fig. 5). Foil and flywheel masses and inertia, and flywheel damper values were chosen as for [2]. Time histories of reduced frequency $k = \omega c / U_\infty$ and power coefficient due to aerodynamic forces and moments $C_{Paero} = C_L \dot{y} / U_\infty + C_M \dot{\theta} c / U_\infty$ are shown in Fig. 6. Here it should be noted that the circular frequency of the system ω is identical to the flywheel rotation rate β , which is not constant as in prescribed motion studies. There is only a very small effect apparent in the power from the change from discontinuous to continuous second derivative, and this is reflected in the very similar reduced frequency (i.e. non-dimensional flywheel rate) time histories.

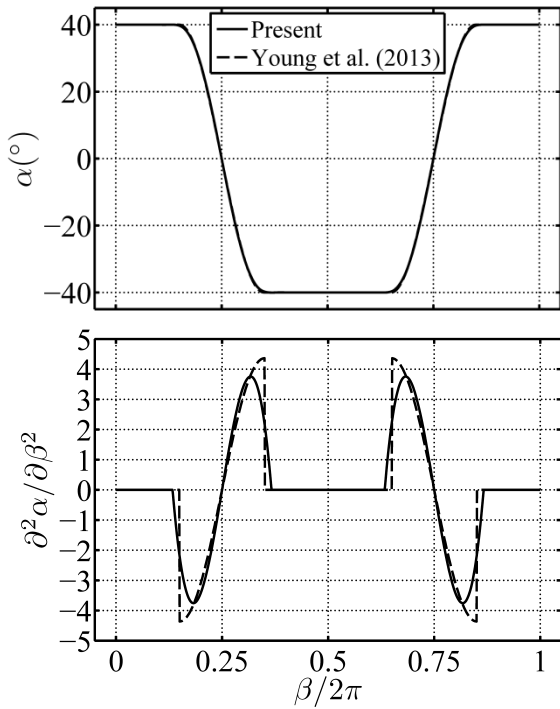


Fig. 5. Comparison of α and $\alpha_{\beta\beta}$ profiles, for the optimum case of Young et al. [2], and the present baseline case ($\delta = 0.5337$, $\mu = 0$, $\gamma = 0$).

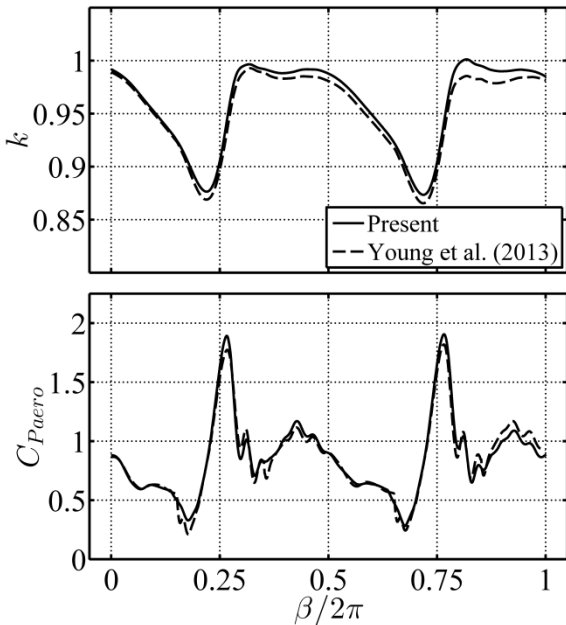


Fig. 6. Comparison of reduced frequency $k = \omega c/U_\infty = \beta c/U_\infty$ and $C_{paero} = C_L \dot{y}/U_\infty + C_M \dot{\theta} c/U_\infty$, for the optimum case of Young et al. [2], and the present baseline case ($\delta = 0.5337$, $\mu = 0$, $\gamma = 0$, $\alpha_e = 53.676^\circ$).

4.2 Variation of Phase Angle ϕ

The phase angle ϕ by which the angle of attack profile leads the plunge motion was first

varied from the baseline case. Results are shown in Fig. 7.

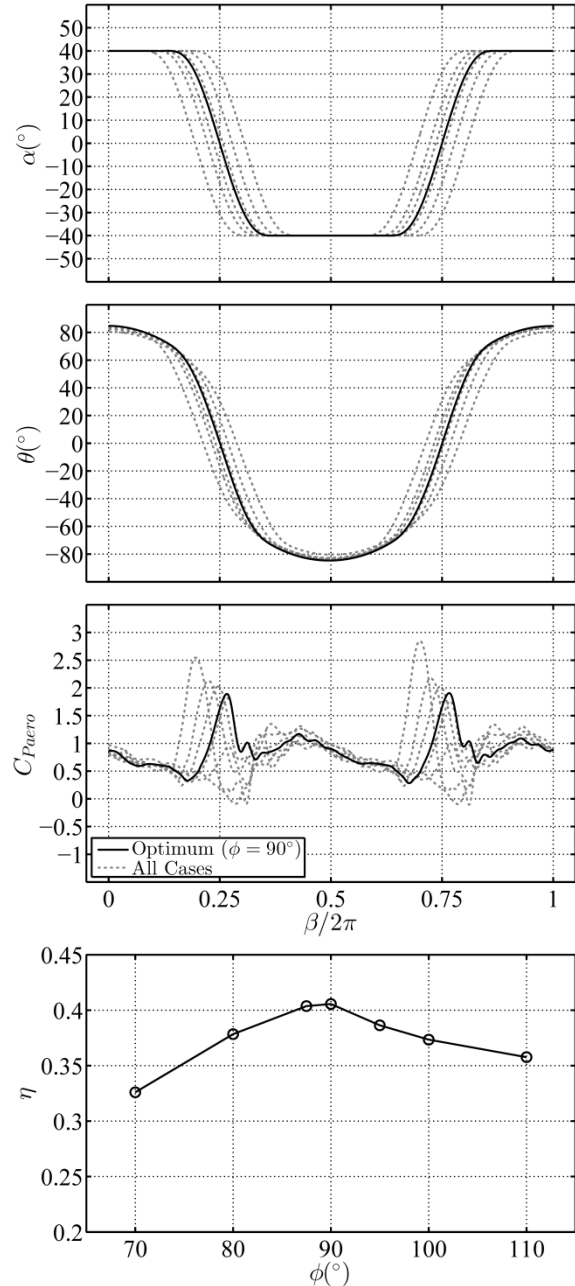


Fig. 7. Comparison of α profiles, resulting θ profiles, $C_{paero} = C_L \dot{y}/U_\infty + C_M \dot{\theta} c/U_\infty$ and efficiency η versus phase ϕ ($\delta = 0.5337$, $\mu = 0$, $\gamma = 0$, $\alpha_e = 53.676^\circ$).

There is a clear peak in efficiency centred around a phase of $\phi = 90^\circ$ (the baseline case). The power coefficient plot shows that this phase value does not generate the highest power at any given time. Indeed higher phases (α leading y by a greater amount) generate larger peaks in power at the middle of stroke reversal, as the leading edge vortex (with an attendant low

pressure region) interacts with the trailing edge and causes a large pitching moment in the direction of foil rotation (see [2] for details of this mechanism). However the timing of the interaction is crucial as once the foil has completed stroke reversal and translates, this low pressure opposes the motion and causes a dip in power, which for the higher phases more than offsets the earlier high power in the time-average used to measure efficiency.

4.3 Variation of Slope Parameter μ

Next the effect of the slope of the angle of attack profile in the periods outside the stroke reversal was considered, to investigate whether the leading edge vortex behaviour could be influenced. A phase of $\phi = 90^\circ$ was used for all cases here. Results are shown in Fig. 8. Interestingly there is a broad region of high efficiency, where the slope has only a moderate effect on time-average performance.

The flow field is visualised in Fig. 9 for four cases, $\mu = 0.0, 0.025, 0.2$ (high efficiency) and -0.1 (lower efficiency) at four different times in the stroke, as the foil reverses direction. For the three high efficiency cases the vortex structure is largely similar throughout the stroke reversal. A large leading edge vortex is generated, and moves past the trailing edge just after the mid-point of stroke reversal ($\beta/2\pi = 0.26$). There are minor variations in the size and positioning of the vortex relative to the foil. There is a marginal benefit at $\mu = 0.025$ compared to the remainder of cases.

In contrast, for the lower efficiency case ($\mu = -0.1$) the timing of vortex formation and interaction is quite different. Here the leading edge vortex has already moved past the trailing edge by $\beta/2\pi = 0.22$, and is thus too early to contribute a strong beneficial pitching moment. By $\beta/2\pi = 0.26$ it has induced a strong counter-rotating vortex from the trailing edge which contributes a low pressure opposing the foil translational motion once stroke reversal is

complete, leading to a loss in power as shown in Fig. 8.

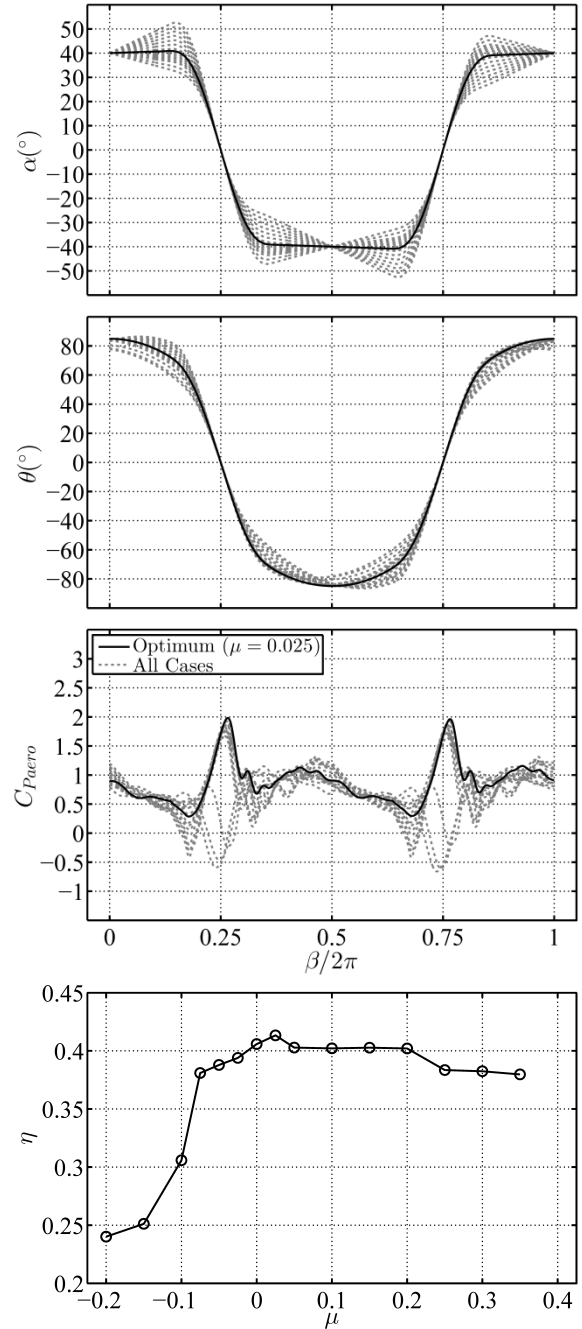


Fig. 8. Comparison of α profiles, resulting θ profiles, $C_{paero} = C_L \dot{y}/U_\infty + C_M \dot{\theta} c/U_\infty$ and efficiency η versus slope μ ($\delta = 0.5337, \gamma = 0, \alpha_e = 53.676^\circ, \phi = 90^\circ$).

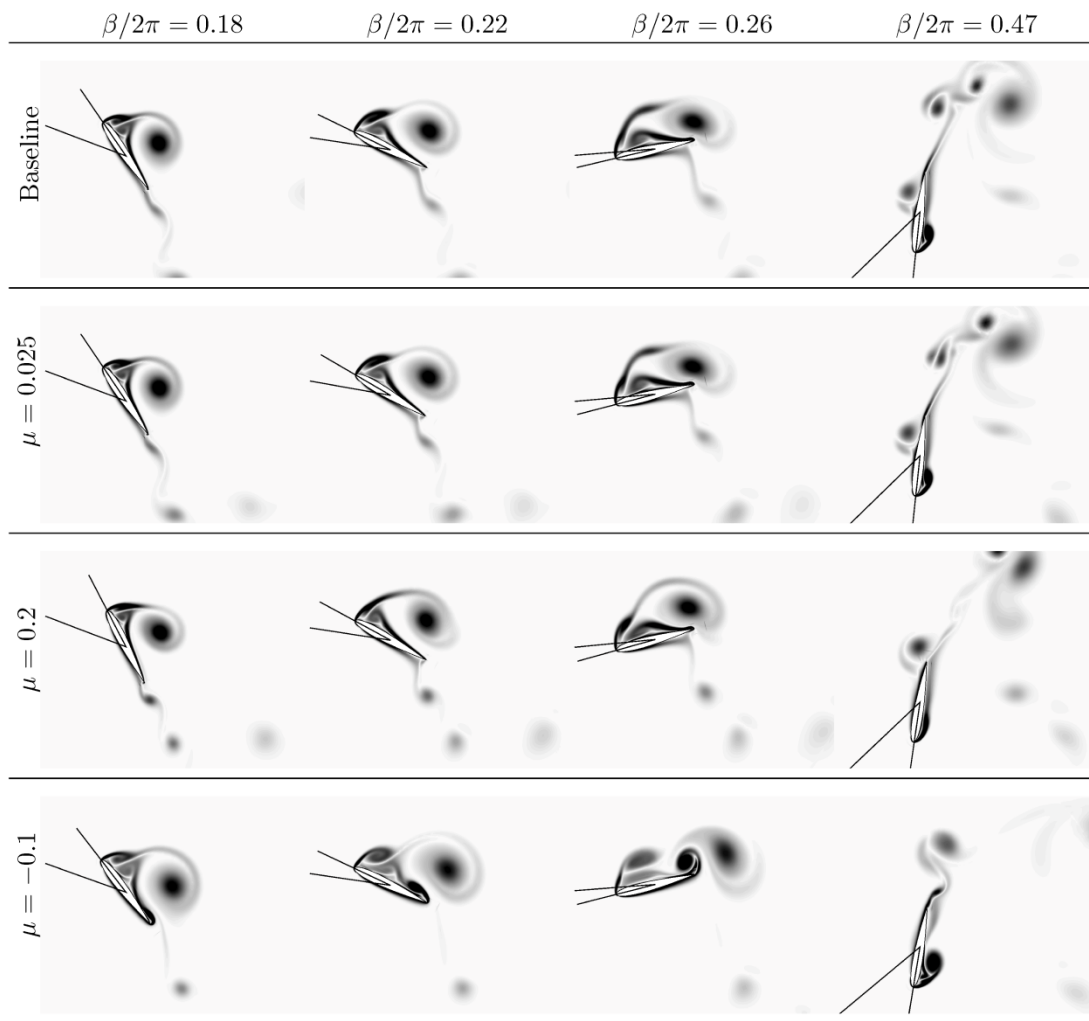


Fig. 9. Vorticity magnitude during and after stroke reversal, for four different slope parameter values. Instantaneous angle of attack on the foil is indicated by black lines.

4.4 Variation of Curvature Parameter γ

Finally the effect of the curvature parameter in the periods outside the stroke reversal was assessed, as shown in Fig. 10. All cases here used phase $\phi = 90^\circ$, and two different slope parameters were considered, $\mu = 0.0$ and $\mu = 0.2$.

Once again there is a much lesser effect on efficiency than for variation in phase. The performance is also less sensitive to the curvature parameter than to the slope parameter, in that the performance is maintained across a wide range of γ values, both positive and negative.

The flow field is visualised in Fig. 11 for three cases, namely the baseline case again

($\gamma = 0.0$) and positive and negative curvatures ($\gamma = 0.6$ and $\gamma = -0.4$). A similar link between vortex structure and time-average performance is revealed here, in comparison to Fig. 9. While the leading edge vortex formation is broadly the same for the three cases shown in Fig. 11, minor differences in size and timing of formation of the vortex lead to variations in the interaction of the vortex with the foil, which in turn leads to changes in the power coefficient peaks during stroke reversal shown in Fig. 10. This is most apparent for $\gamma = -0.4$, where there the vortex moves past the trailing edge earlier in the cycle than for $\gamma = 0.0$, and a secondary vortex is induced in the same way as discussed for $\mu = -0.1$ in Fig. 9 (although the effect is not as pronounced here).

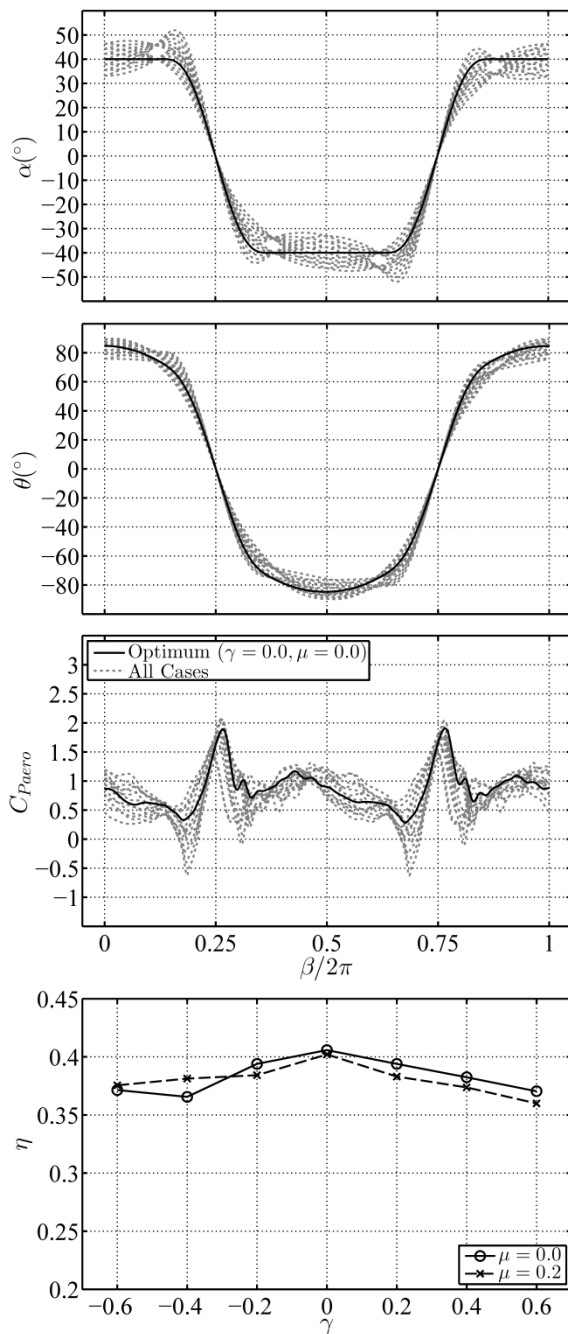


Fig. 10. Comparison of α profiles, resulting θ profiles, $C_{p_{aero}} = C_L \dot{\gamma} / U_\infty + C_M \dot{\theta} c / U_\infty$ and efficiency η versus curvature γ ($\delta = 0.5337$, $\mu = 0.0$ and 0.2 , $\alpha_e = 53.676^\circ$, $\phi = 90^\circ$).

5 Conclusions

The results of this work show that the power generation of a passive flapping foil system can be sensitive to some variations in the angle of attack profile, and relatively robust to others, at least at the Reynolds number under consideration here (1100). Changes in the phase between the angle of attack profile and the

plunge motion produced the largest variations in efficiency, indicating that the timing of the formation of the leading edge vortex is one of the most important considerations. Not only does the timing affect the size of the vortex produced, but also the interactions with the foil and in what manner the foil is moving when those interactions take place (thus determining whether instantaneous power contributions are positive or negative).

Once a single phase had been chosen ($\phi = 90^\circ$), other changes in the profile generated by variations in slope and curvature parameters μ and γ had a lesser effect across a broad parameter value range. As these results are governed chiefly by the leading edge vortex, high Reynolds number turbulent flow may produce significantly different behaviour and this remains to be investigated.

6 Contact Author Email Address

j.young@adfa.edu.au

Copyright Statement

The authors confirm that they, and/or their company or organization, hold copyright on all of the original material included in this paper. The authors also confirm that they have obtained permission, from the copyright holder of any third party material included in this paper, to publish it as part of their paper. The authors confirm that they give permission, or have obtained permission from the copyright holder of this paper, for the publication and distribution of this paper as part of the ICAS 2014 proceedings or as individual off-prints from the proceedings.

References

- [1] Young J, Lai JCS, and Platzer MF. A Review of Progress and Challenges in Flapping Foil Power Generation. *Progress in Aerospace Sciences*, in press, 2014. doi: 10.1016/j.paerosci.2013.11.001
- [2] Young J, Ashraf MA, Lai JCS, and Platzer MF. Numerical simulation of fully passive flapping foil power generation. *AIAA Journal* Vol. 51 No. 11, pp. 2727-2739, 2013. doi: 10.2514/1.J052542
- [3] Kinsey T and Dumas G. Computational fluid dynamics analysis of a hydrokinetic turbine based on oscillating hydrofoils. *Journal of Fluids Engineering* Vol. 134, pp. 021104, 2012. doi: 10.1115/1.4005841
- [4] Zhu, Q. Energy harvesting by a purely passive flapping foil from shear flows. *Journal of Fluids and*

- Structures* Vol. 34, pp. 157-169, 2012. doi: 10.1016/j.jfluidstructs.2012.05.013
- [5] McKinney W and DeLaurier J. Wingmill: An oscillating-wing windmill. *Journal of Energy* Vol. 5, pp. 109-115, 1981. doi: 10.2514/3.62510
- [6] Usuh CO, Young J, Lai JCS and Ashraf MA. Numerical analysis of a non-profiled plate for flapping wing turbines. *18th Australasian Fluid Mechanics Conference*, Launceston, Australia, 3-7 December 2012.
- [7] Kloos G, Gonzalez CA and Finnigan TD. The BioSTREAM Tidal Current Energy Converter. *European Wave and Tidal Conference (EWTEC)*, Uppsala, Sweden, 2009.
- [8] Zhu Q, Haase M, and Wu CH. Modeling the capacity of a novel flow energy harvester. *Applied Mathematical Modelling* Vol. 33, pp. 2207-2217, 2009. doi: 10.1016/j.apm.2008.05.027
- [9] Peng Z and Zhu Q. Energy harvesting through flow-induced oscillations of a foil. *Physics of Fluids* Vol. 21 No. 12, pp. 123602, 2009. doi: 10.1063/1.3275852
- [10] Young J, Ashraf MA, Lai JCS and Platzer MF. Numerical Simulation of Flow-Driven Flapping-Wing Turbines for Wind and Water Power Generation. *17th Australasian Fluid Mechanics Conference*, Auckland, New Zealand, 5-9 December, 2010.
- [11] Kinsey T, Dumas G, Lalande G, Ruel J, Mhut A, Viarouge P, Lemay J, and Jean Y. Prototype testing of a hydrokinetic turbine based on oscillating hydrofoils. *Renewable Energy* Vol. 36 No. 6, pp. 1710-1718, 2011. doi: 10.1016/j.renene.2010.11.037
- [12] Ashraf MA, Young J, Lai JCS and Platzer MF. Numerical Analysis of an Oscillating-Wing Wind and Hydropower Generator. *AIAA Journal* Vol. 49 No. 7, pp. 1374-1386, 2011. doi: 10.2514/1.J050577
- [13] Platzer MF, Ashraf MA, Young J and Lai JCS. Development of a New Oscillating-Wing Wind and Hydropower Generator. *47th AIAA Aerospace Sciences Meeting*, 2009.
- [14] Xiao Q, Liao W, Yang S and Peng Y. How motion trajectory affects energy extraction performance of a biomimic energy generator with an oscillating foil. *Renewable Energy* Vol. 37 No. 1, pp. 61-75, 2012. doi: 10.1016/j.renene.2011.05.029
- [15] Hover FS, Haugsdal A and Triantafyllou MS. Effect of angle of attack profiles in flapping foil propulsion. *Journal of Fluids and Structures* Vol. 19 No. 1, pp. 37-47, 2004. doi: 10.1016/j.jfluidstructs.2003.10.003
- [16] Jones KD, Lund TC and Platzer MF. Experimental and computational investigation of flapping wing propulsion for micro air vehicles. *Fixed and Flapping Wing Aerodynamics for Micro Air Vehicle Applications*, Mueller TJ (ed.), AIAA, pp. 307-399, 2001.
- [17] Kinsey T and Dumas G. Parametric study of an oscillating airfoil in a power-extraction regime. *AIAA Journal* Vol. 46 No. 6, pp. 1318-1330, 2008. doi: 10.2514/1.26253

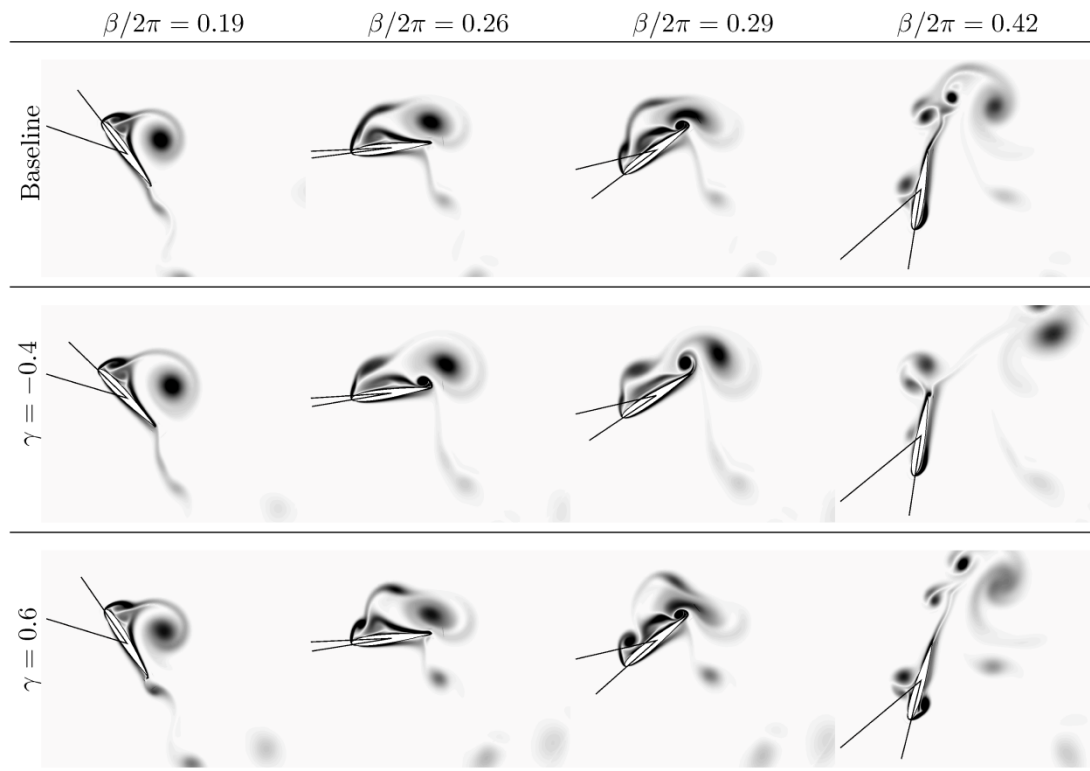


Fig. 11. Vorticity magnitude during and after stroke reversal, for three different curvature parameter values, with slope $\mu = 0.0$. Instantaneous angle of attack on the foil is indicated by black lines.

